Supporting Information for: Probing crystal structures of dicarbamate phase change materials to inform structural design

Samantha L. Piper,[a] Craig M. Forsyth,[a] Mega Kar,[b] Luke A. O'Dell,[b] Jisheng Ma,[c] Jennifer M. Pringle,[b] Douglas R. MacFarlane[a] and Karolina Matuszek*[a]

[a]*School of Chemistry, Monash University, Clayton, Victoria 3800, Australia.*

[b]*Institute for Frontier Materials, Deakin University, Burwood Campus, Burwood, Victoria 3125, Australia.*

[c] *Monash X-ray Platform & Department of Materials and Engineering, Monash University, Clayton, Victoria 3800, Australia.*

Table of Contents

Table of Figures

1. Single-crystal X-ray crystallography

Data for C18-cyhx, C18-Ph and C18-MePh was collected at 100 K on the Micro Crystallography – MX2 beamline at the Australian Synchrotron.[1] The data collection and integration were performed within the Blu-Ice[2] and XDS software programs.[3] The structures were solved and refined using the SHELX[4,5] software suite, and refined against F^2 using Olex2[6] as a graphical interface. Alkyl hydrogen atoms were placed in calculated positions using the riding model, and the urethane N-H protons were modelled based on electron density, with restrained N-H bond lengths of 0.91(2) using the DFIX restraint.

For C18-MePh, two datasets were merged using XPREP, program of the SHELX software suite. The structure was solved in the orthorhombic $Pmc2_1$ space group with two half molecules in the asymmetric unit. Two other space group solutions were considered feasible for this

structure: the centrosymmetric *Pbcm*, for which the solution contained one half molecule in the asymmetric unit, and non-centrosymmetric $Pca2_1$, for which the solution contained one whole molecule per asymmetric unit. The $Pmc2_1$ solution was considered the most appropriate based on anisotropic displacement parameters and R values.

In the structure of C18-MePh, the urethane groups in both half molecules were modelled as disordered over two positions, with fixed occupancies of 0.5. Bonds from the disordered components were restrained to the same length as the corresponding bonds from the second components, using the SADI restraint.

The toluene methyl group of both half molecules is modelled with fixed occupancies of 0.5. The corresponding proton attached to the carbon ring in the absence of this methyl group is also fixed to an occupancy of 0.5. The carbon from the toluene ring which bonds to this proton/methyl group was split, and the resulting two carbon atoms were constrained to occupy the same position using the EXYZ constraint. The two equivalent carbons were constrained to the same anisotropic displacement parameters using the EADP constraint. The two nitrogen atoms of the urethane functionalities were also split and constrained to the same anisotropic displacement parameters and position using the EADP and EXYZ constraints, at fixed occupancies of 0.5.

Table S1. Crystal data and structure refinement details for C18-cyhx, C18-Ph and C18-MePh.

Identification code	**C18-cyhx**	**C18-Ph**	**C18-MePh**
CCDC identifier	2259816	2259815	2259817
Empirical formula	$C_{44}H_{86}N_2O_4$	$C_{44}H_{80}N_2O_4$	$C_{45}H_{82}N_2O_4$
Formula weight/g.mol^{-1}	707.14	701.10	715.12
Temperature/K	100(2)	100(2)	100.0(2)
Crystal system	triclinic	triclinic	orthorhombic
Space group	*P*-1	*P*-1	$Pmc2_1$
a/Å	5.1620(10)	5.0750(10)	85.724(17)
b/Å	7.0660(14)	7.2740(15)	4.6340(9)
c/Å	31.039(6)	30.348(6)	10.823(2)
α/°	93.85(3)	93.10(3)	90
β/°	91.53(3)	93.33(3)	90
γ/°	107.76(3)	109.97(3)	90
Volume/Å^3	1074.4(4)	1047.9(4)	4299.4(15)
Z	1	1	4
***p* calc/g/cm^3**	1.093	1.111	1.105
μ/mm^{-1}	0.068	0.069	0.069
F(000)	396.0	390.0	1592.0
Crystal size/mm^3	0.08 × 0.02 × 0.01	0.06 × 0.02 × 0.01	0.2 × 0.01 × 0.01
Radiation	Synchrotron (λ = 0.71091)	Synchrotron (λ = 0.71075)	Synchrotron (λ = 0.710764)
2Θ range for data collection/°	2.634 to 64.066	2.696 to 63.938	1.426 to 52
Index ranges	-6 ≤ h ≤ 6, -9 ≤ k ≤ 9, -43 ≤ l ≤ 43	-6 ≤ h ≤ 6, -10 ≤ k ≤ 10, -43 ≤ l ≤ 44	-105 ≤ h ≤ 105, -5 ≤ k ≤ 5, -13 ≤ l ≤ 13

Reflections collected	17963	9534	119454
Independent reflections	5383 [R_{int} = 0.0462, R_{sigma} = 0.0474]	5301 [R_{int} = 0.1380, R_{sigma} = 0.1879]	8463 [R_{int} = 0.1154, R_{sigma} = 0.0562]
Data/restraints/parameters	5383/1/231	5301/1/231	8463/11/513
Goodness-of-fit on F2	1.036	0.909	1.072
Final R indexes [I>=2σ (I)]	R_1 = 0.0556, wR_2 = 0.1622	R_1 = 0.0980, wR_2 = 0.2374	R_1 = 0.0911, wR_2 = 0.2813
Final R indexes [all data]	R_1 = 0.0616, wR_2 = 0.1710	R_1 = 0.1438, wR_2 = 0.2921	R_1 = 0.0978, wR_2 = 0.2899
Largest diff. peak/hole / e Å^{-3}	0.36/-0.25	0.35/-0.35	0.40/-0.40
Flack parameter	-	-	-0.4(10)

Table S2. Distances and angles of hydrogen bonds in C18-hx, C18-MDP, C18-cyhx, C18-Ph and C18-MePh.

Compound	**Donor**	**Proton**	**Acceptor**	**D-H (Å)**	**H···A (Å)**	**D···A (Å)**	**D-H···A(°)**
C18-hx[7]	N1	H1	O2	0.899(15)	1.983(15)	2.880(2)	175.1(19)
C18-MDP[7]	N1	H1	O1	0.84(2)	2.10(4)	2.909(4)	161(3)
C18-cyhx	N1	H1	O2	0.867(11)	2.165(11)	3.0041(11)	162.8(11)
C18-Ph	N1	H1	O2	0.913(16)	2.080(17)	2.903(2)	149.4(19)
C18-MePh	N1[a]	H1A[a]	O1[a]	0.88	2.07	2.930(7)	163.7
	N1'[b]	H1B[b]	O1[b]	0.88	2.00	2.864(7)	166.2
	N2[a]	H2A[a]	O3[a]	0.88	2.06	2.934(9)	171.4
	N2'[b]	H2B[b]	O3[b]	0.88	1.93	2.803(9)	174.7

3. Powder X-ray diffraction

3.1 Ambient temperature powder X-ray diffraction

Ambient powder X-ray diffraction patterns of all samples were collected at room temperature on a Bruker D8 Advance equipped with Cu-Kα radiation (λ = 1.54 Å). A step time of 0.1 s was used with a step size of 0.021°.

3.2 In situ powder X-ray diffraction

For *in situ* powder X-ray diffraction experiments, samples were loaded on an MTC wide range temperature controlling stage and experiments were conducted under a dried nitrogen atmosphere using a Bruker D8 Advance equipped with Cu-Kα radiation (λ = 1.54 Å). A step time of 0.2 s was used with a step size of 0.021°. For C18-cyhx, the sample was heated at a rate of 5 °C min^{-1} and held at each temperature for five minutes prior to the beginning of the scan. The C18-MePh sample was heated at a rate of 1 °C min^{-1}, to replicate the conditions of

the 1 °C min^{-1} DSC scan. The sample was held at each target temperature for 5 minutes prior to the commencement of each scan.

3. Static solid-state nuclear magnetic resonance spectroscopy (NMR)

3.1 Experimental method

Static solid-state ^{1}H NMR experiments were conducted on a Bruker Avance III wide-bore spectrometer equipped with a 11.7 T magnet and 5 mm static HX variable-temperature probe, operating at 500.07 MHz (^{1}H frequency). Samples were packed in a 5 mm glass tube, and the spectra were recorded with single-pulse excitation over 16 scans with a relaxation delay of 5 seconds and pulse width of 3 µs. Frequency scales were referenced to the signal of a tetramethylsilane standard (0 kHz). Spectra were analysed using Topspin and deconvolution fitting was done with the DMfit software. For consistency, fitting was restricted to two (broad and narrow) components representing less and more dynamic protons respectively. Additional peak intensity observed to the left of the narrow component is attributed to chemical shift effects (*i.e.,* deshielding of the protons close to the carbamate groups).

3.2 Static solid-state NMR spectra of C18-cyhx and C18-MePh, deconvoluted

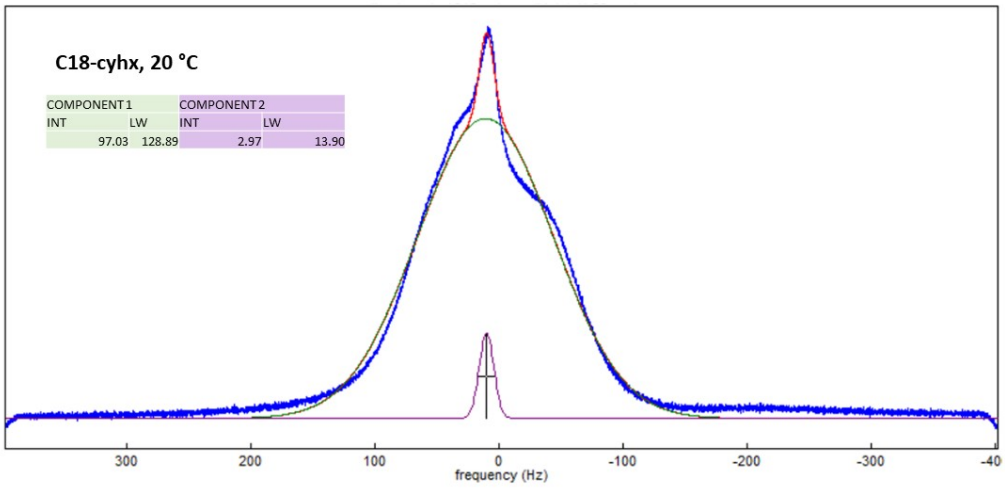

Figure S1. Solid-state NMR spectrum of C18-cyhx collected at 20 °C, deconvoluted using DMfit software. The line width and integration of each component is shown in the inset table.

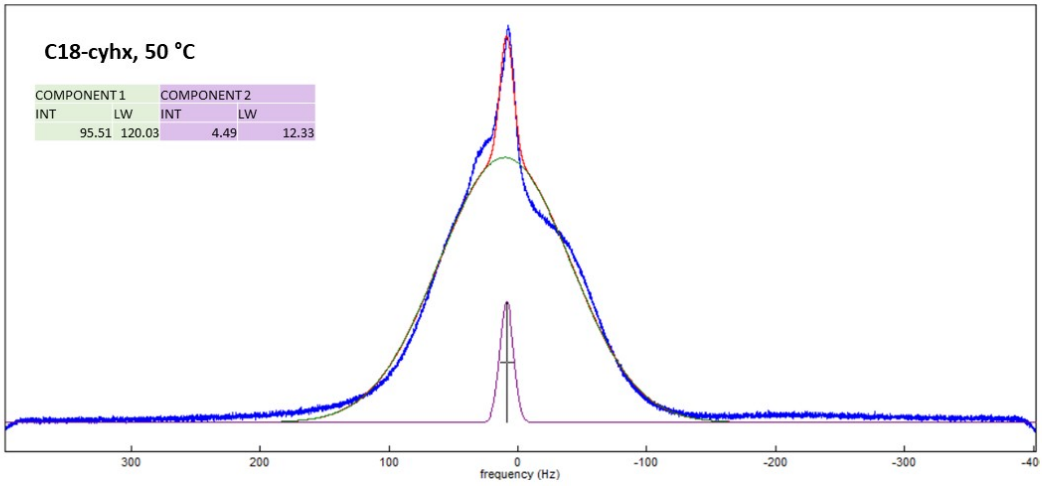

Figure S2. Solid-state NMR spectrum of C18-cyhx collected at 50 °C, deconvoluted using DMfit software. The line width and integration of each component is shown in the inset table.

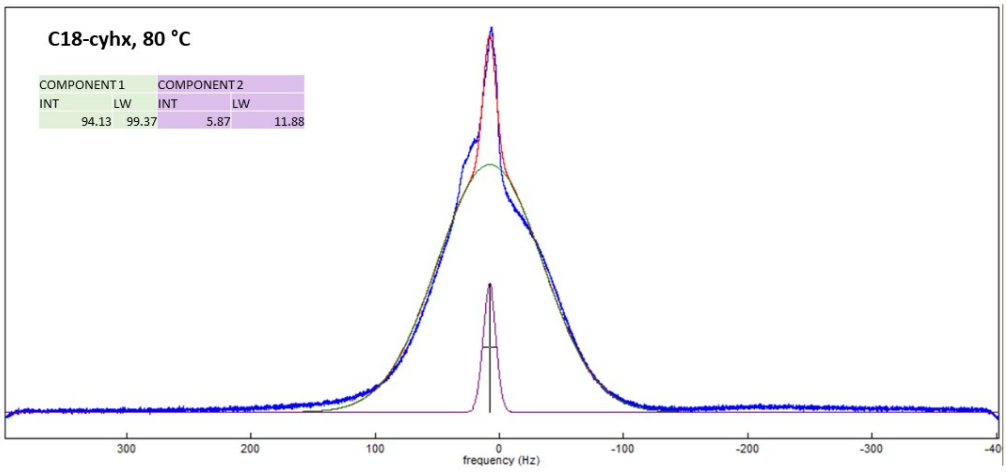

Figure S3. Solid-state NMR spectrum of C18-cyhx collected at 80 °C, deconvoluted using DMfit software. The line width and integration of each component is shown in the inset table.

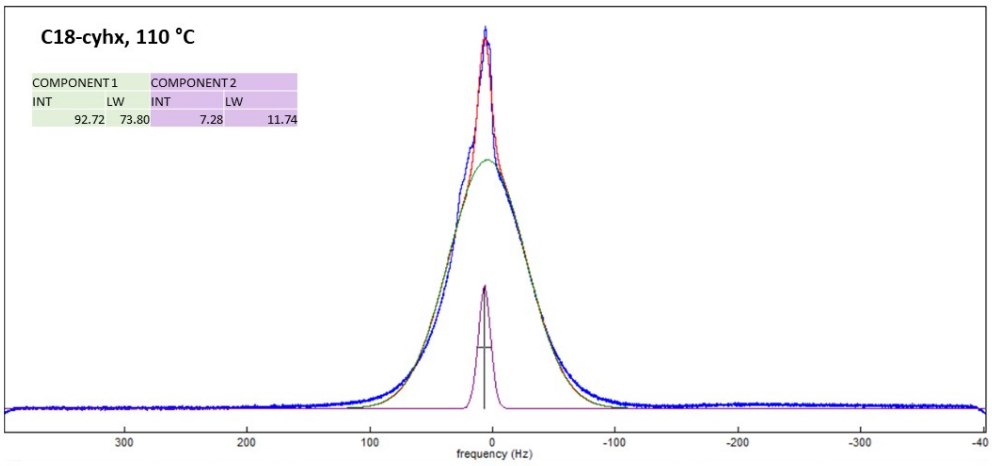

Figure S4. Solid-state NMR spectrum of C18-cyhx collected at 110 °C, deconvoluted using DMfit software. The line width and integration of each component is shown in the inset table.

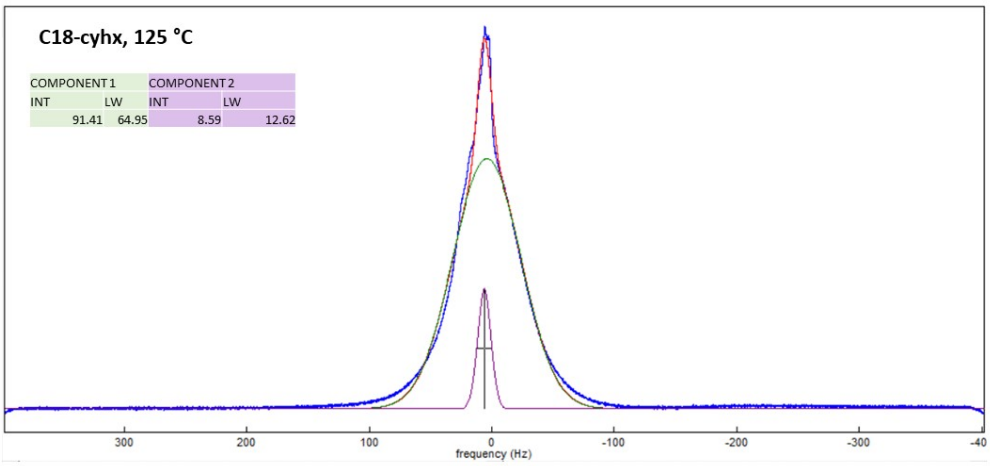

Figure S5. Solid-state NMR spectrum of C18-cyhx collected at 125 °C, deconvoluted using DMfit software. The line width and integration of each component is shown in the inset table.

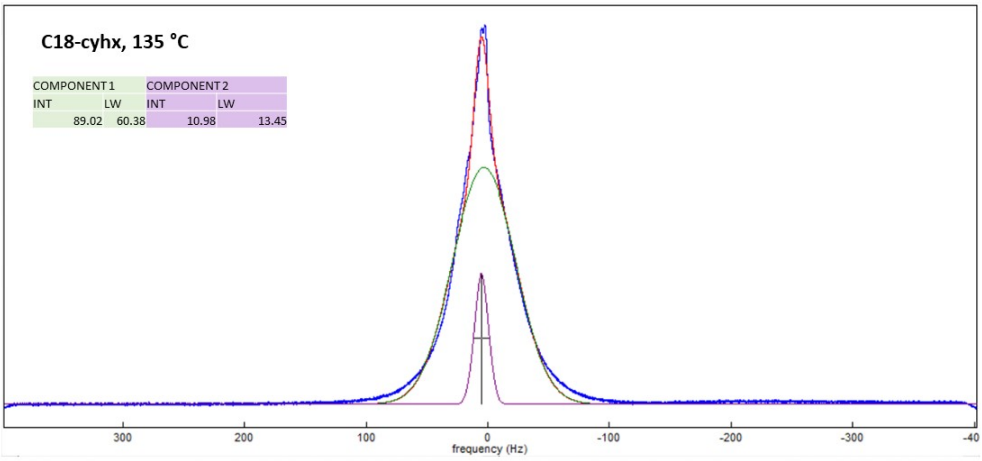

Figure S6. Solid-state NMR spectrum of C18-cyhx collected at 135 °C, deconvoluted using DMfit software. The line width and integration of each component is shown in the inset table.

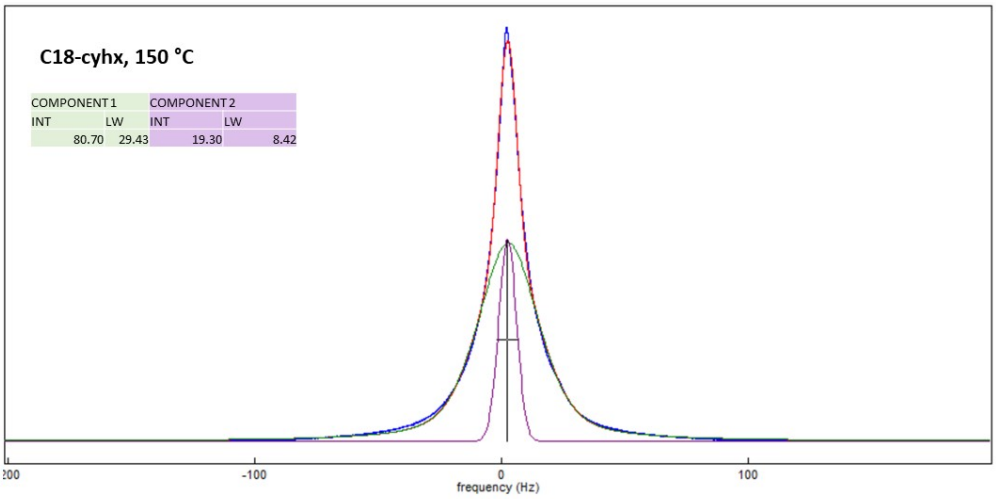

Figure S7. Solid-state NMR spectrum of C18-cyhx collected at 150 °C, deconvoluted using DMfit software. The line width and integration of each component is shown in the inset table.

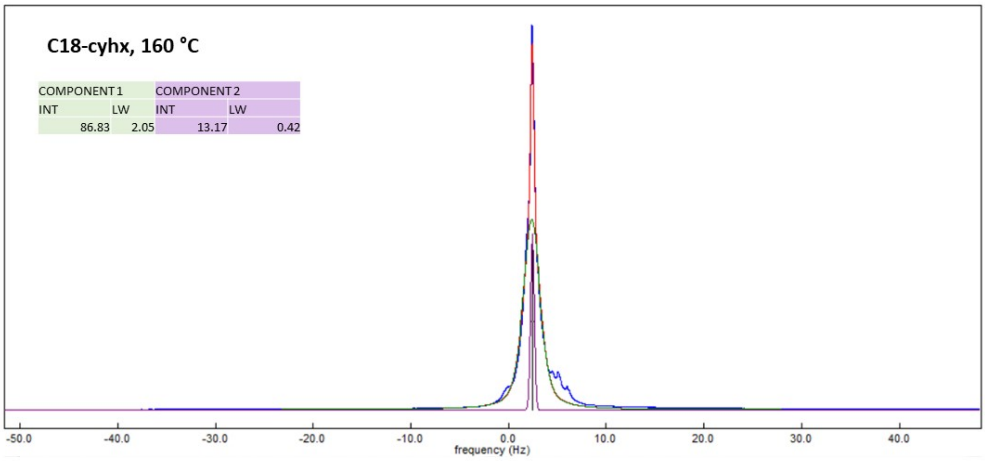

Figure S8. Solid-state NMR spectrum of C18-cyhx collected at 160 °C, deconvoluted using DMfit software. The line width and integration of each component is shown in the inset table.

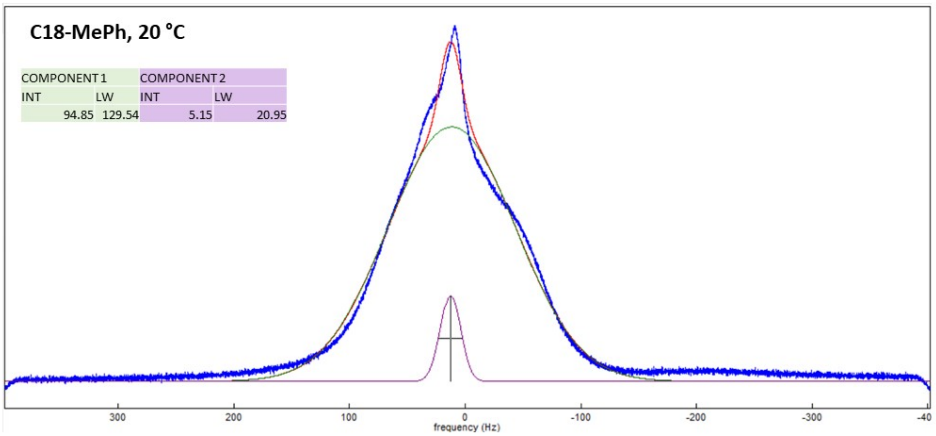

Figure S9. Solid-state NMR spectrum of C18-MePh collected at 20 °C, deconvoluted using DMfit software. The line width and integration of each component is shown in the inset table.

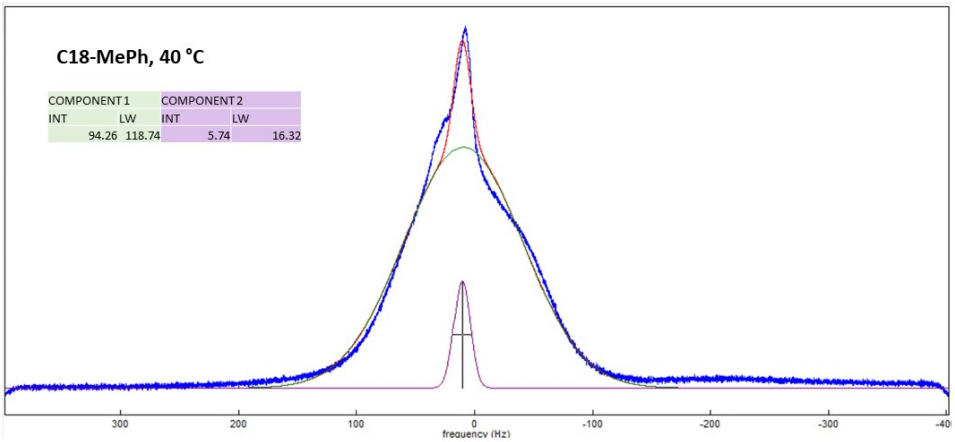

Figure S10. Solid-state NMR spectrum of C18-MePh collected at 40 °C, deconvoluted using DMfit software. The line width and integration of each component is shown in the inset table.

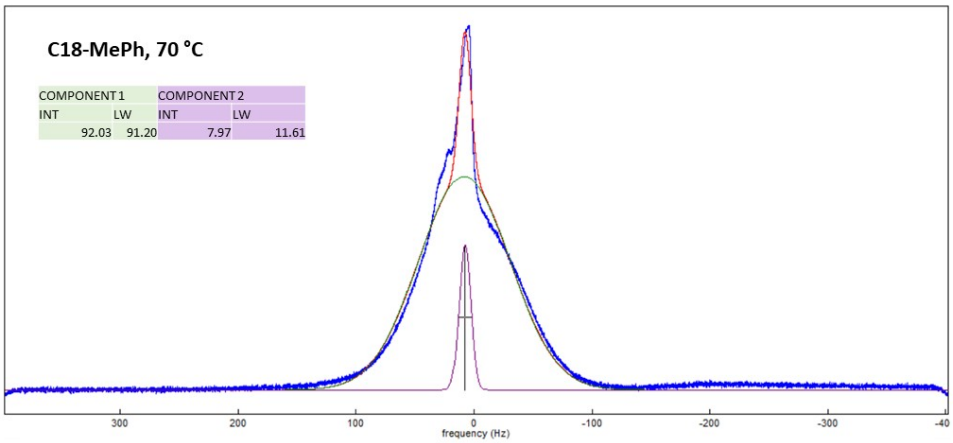

Figure S11. Solid-state NMR spectrum of C18-MePh collected at 70 °C, deconvoluted using DMfit software. The line width and integration of each component is shown in the inset table.

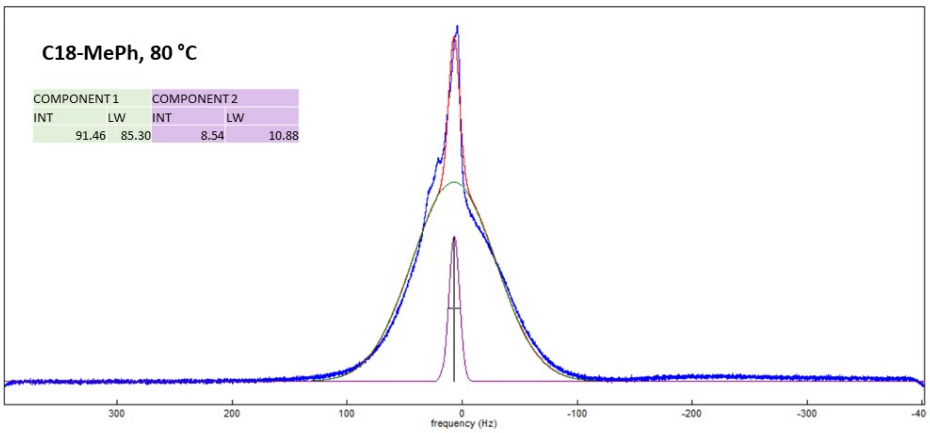

Figure S12. Solid-state NMR spectrum of C18-MePh collected at 80 °C, deconvoluted using DMfit software. The line width and integration of each component is shown in the inset table.

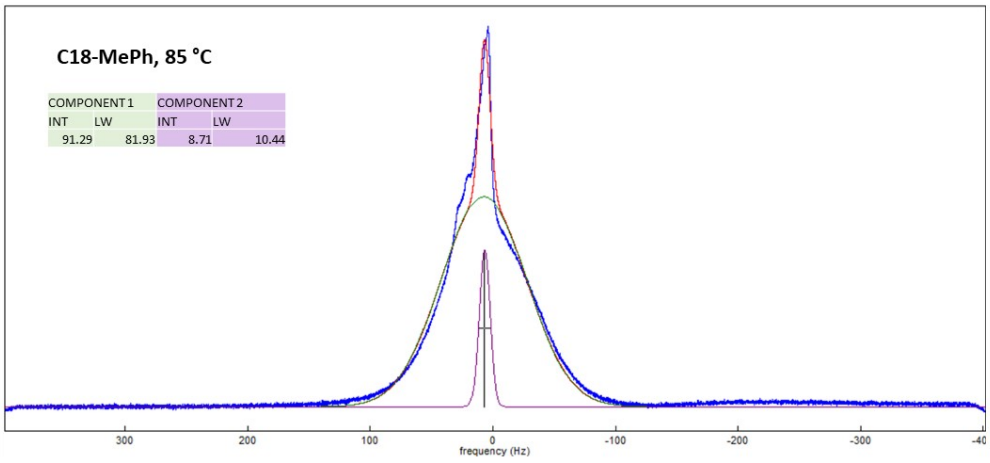

Figure S13. Solid-state NMR spectrum of C18-MePh collected at 85 °C, deconvoluted using DMfit software. The line width and integration of each component is shown in the inset table.

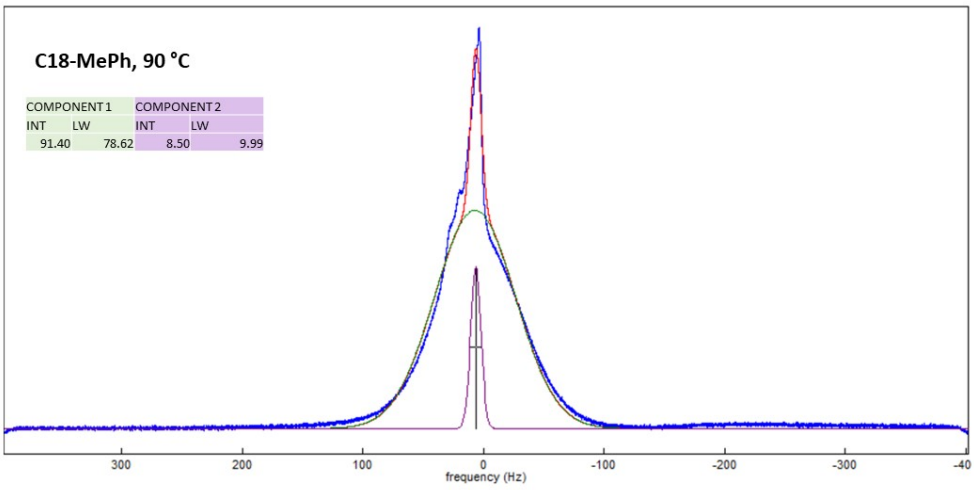

Figure S14. Solid-state NMR spectrum of C18-MePh collected at 90 °C, deconvoluted using DMfit software. The line width and integration of each component is shown in the inset table.

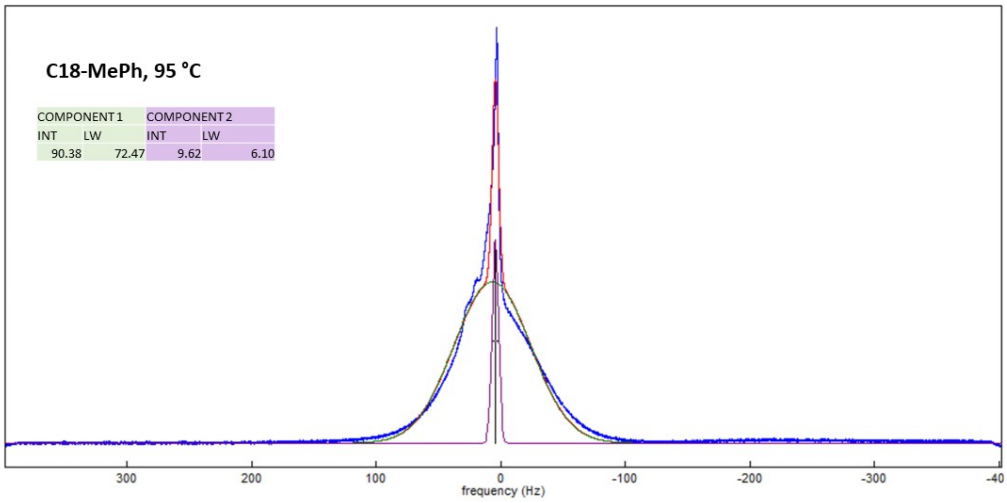

Figure S15. Solid-state NMR spectrum of C18-MePh collected at 95 °C, deconvoluted using DMfit software. The line width and integration of each component is shown in the inset table.

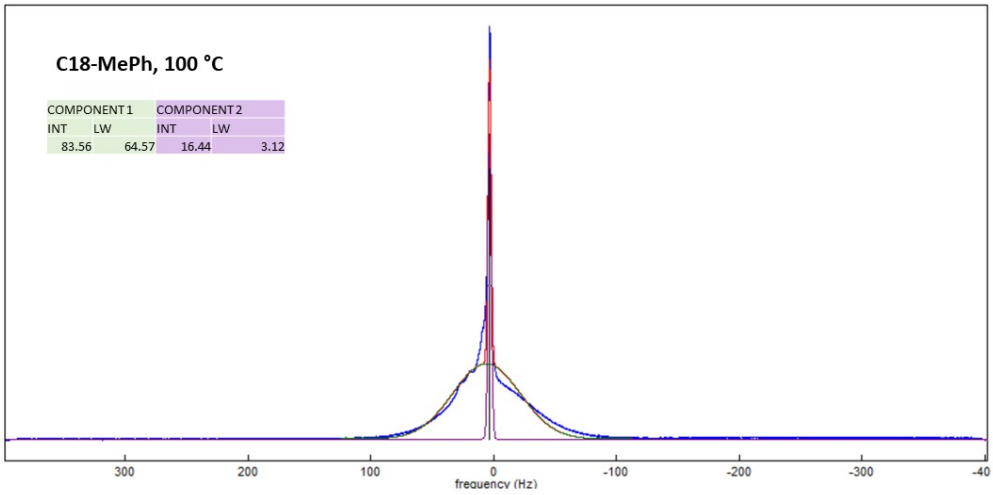

Figure S16. Solid-state NMR spectrum of C18-MePh collected at 100 °C, deconvoluted using DMfit software. The line width and integration of each component is shown in the inset table.

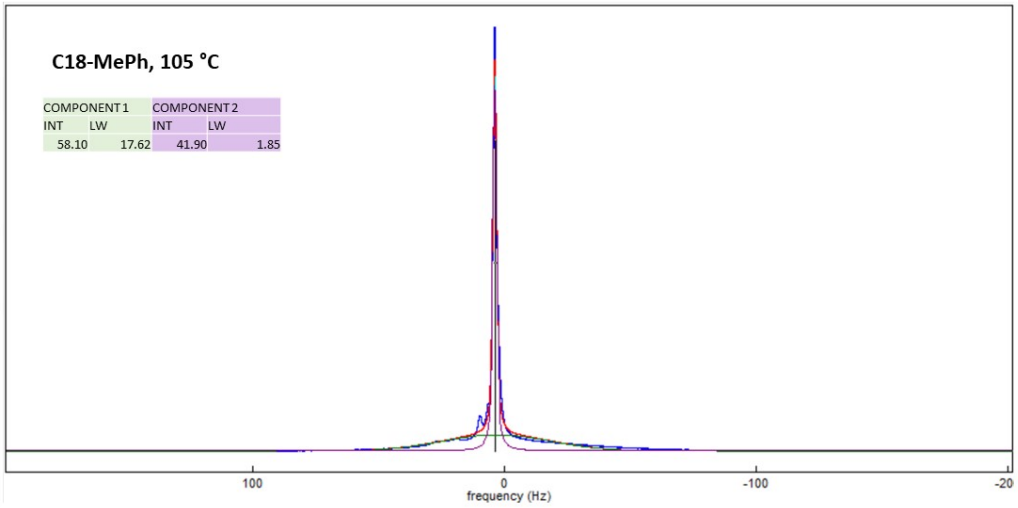

Figure S17. Solid-state NMR spectrum of C18-MePh collected at 105 °C, deconvoluted using DMfit software. The line width and integration of each component is shown in the inset table.

4. C18-MePh thermal properties at different ramp rates, as determined by DSC

The following data is reported from the second heating cycle in DSC experiments, as reported in Ref 7. Figures S18, S19 and S20, below, show all three DSC cycles with the first scan highlighted. The difference in the shape of the first heating scans across the three ramp rates demonstrates that the varying behaviour observed on subsequent cycles is not a result of thermal treatment prior to analysis, as all samples have the same thermal history at the beginning of the experiment.

Table S3. DSC transitions of C18-MePh with a heating and cooling rate of 1 °C min^{-1}.

Transition	T_t **°C**	ΔH_t **J g^{-1}**	ΔH_t **kJ mol^{-1}**	ΔS_t **J mol^{-1} K^{-1}**
exo s-s	94	15	10.7274	29.2180308
Melting	105	140	100.1224	264.769007
Crystallisation (cooling cycle)	83	140	100.1224	281.124245

Table S4. DSC transitions of C18-MePh with a heating and cooling rate of 10 °C min^{-1}.

Transition	T_t **°C**	ΔH_t **J g^{-1}**	ΔH_t **kJ mol^{-1}**	ΔS_t **J mol^{-1} K^{-1}**
Melting	104	112.6	80.527016	213.514559
Endo s-s	85	1	0.71516	1.99681698
Exo s-s	86	2	1.43032	3.98251427
Endo s-s	92	41	29.32156	80.3000411
Exo s-s	95	9	6.43644	17.4831998
Crystallisation (cooling cycle)	133 J g^{-1}, peaks at 75 °C and 69 °C			

Table S5. DSC transitions of C18-MePh with a heating and cooling rate of 20 °C min^{-1}.

Transition	T_t **°C**	ΔH_t **J g^{-1}**	ΔH_t **kJ mol^{-1}**	ΔS_t **J mol^{-1} K^{-1}**
Endo s-s	*67*	*5*	*3.5758*	*10.512421*
Exo s-s	71	14	10.01224	29.0926631
Endo s-s	*80*	*5*	*3.5758*	*10.1254424*
Exo s-s	82	17	12.15772	34.2326341
Endo s-s	*92*	*28*	*20.02448*	*54.8390524*
Exo s-s	95	9	6.43644	17.4831998
Melting	104	115	82.2434	218.065491
Crystallisation (cooling cycle)	120 J g^{-1}, main peak at 60 °C and small shoulder at 68 °C			

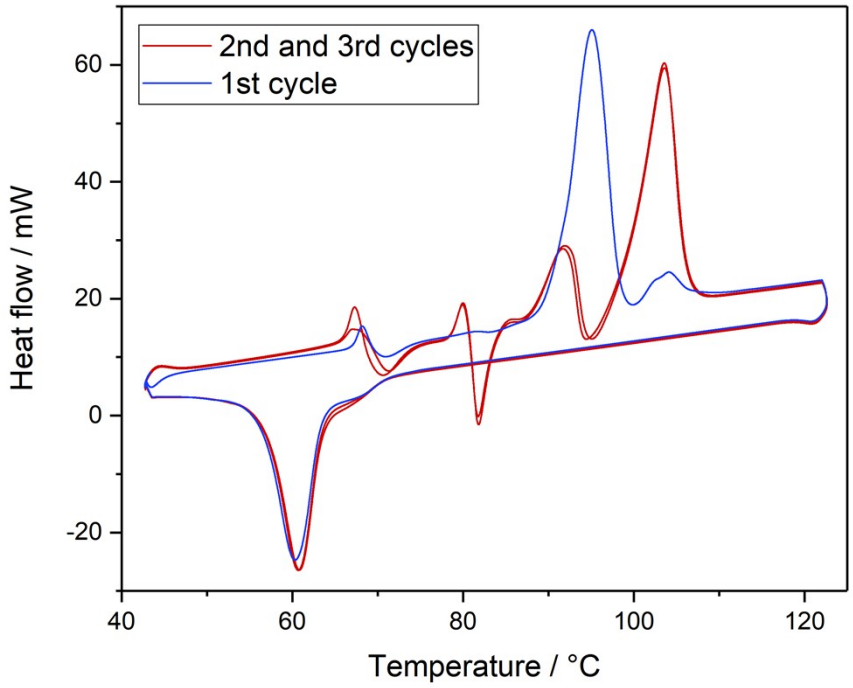

Figure S18. DSC curve of C18-MePh with a ramp rate of 20 °C min^{-1}, as reported in Ref 7.

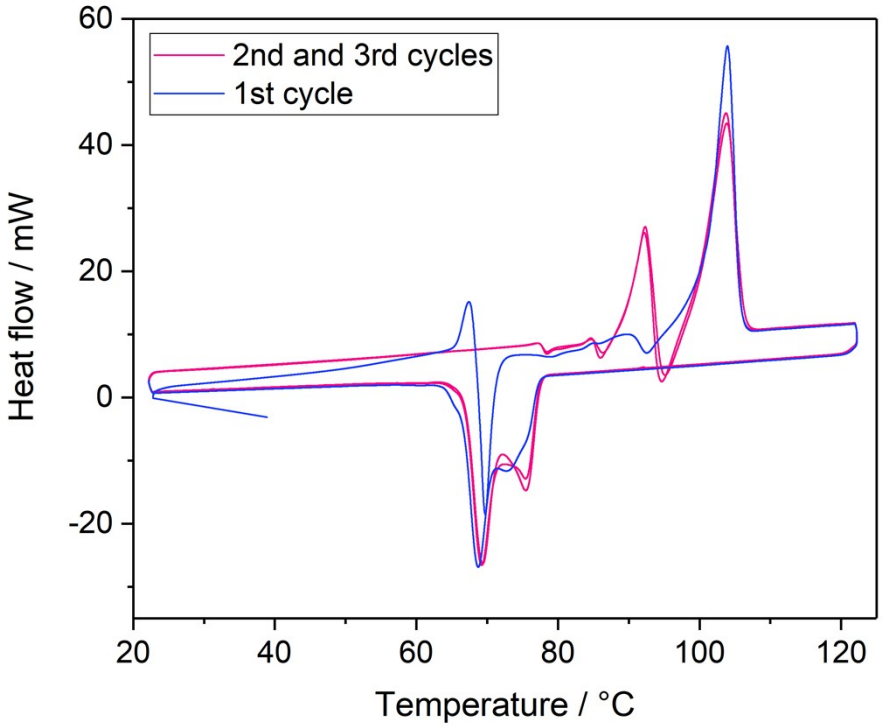

Figure S19. DSC curve of C18-MePh with a ramp rate of 10 °C min^{-1}, as reported in Ref 7.

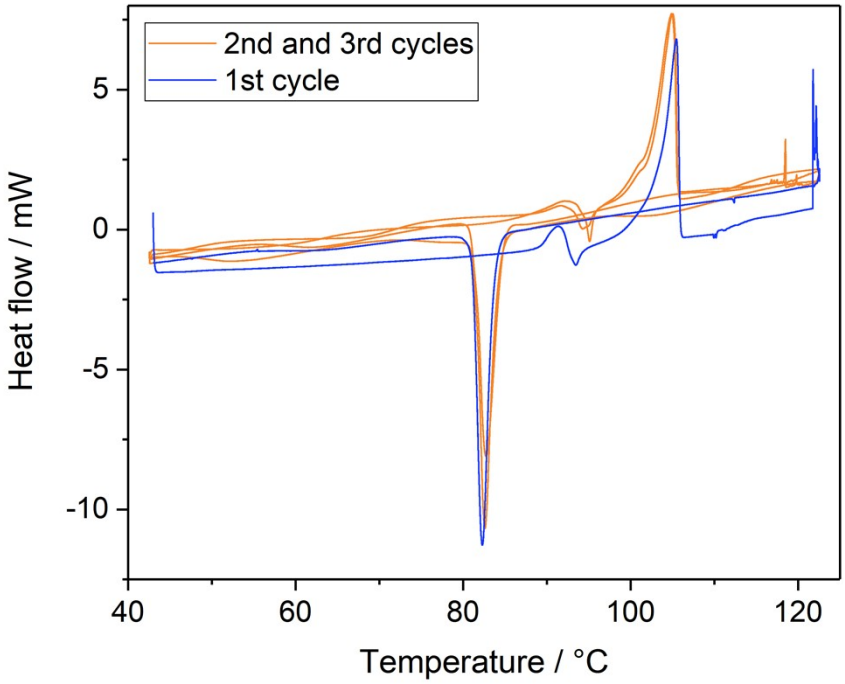

Figure S20. DSC curve of C18-MePh with a ramp rate of 1 °C min^{-1}, as reported in Ref 7.

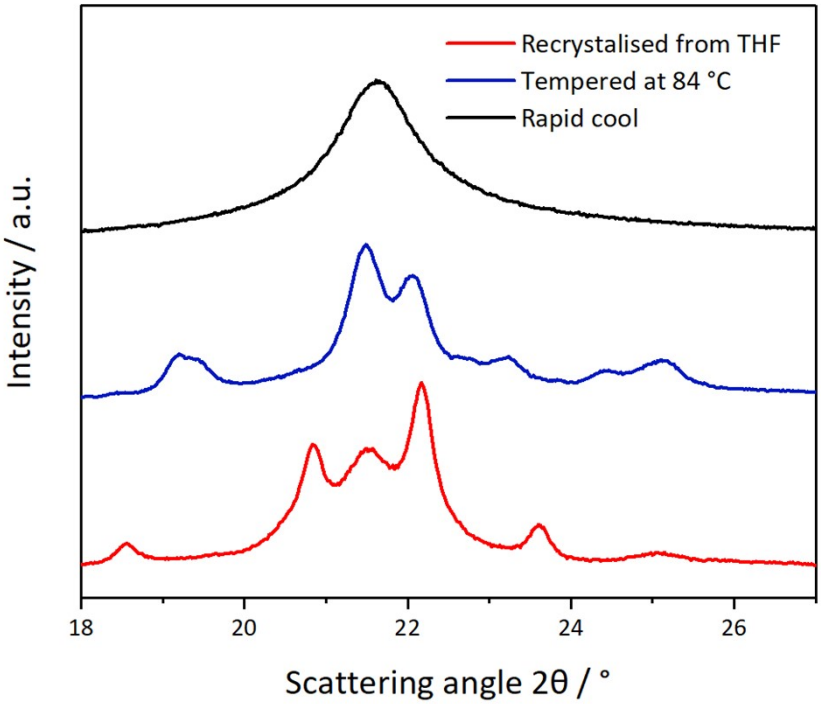

Figure S21. PXRD pattern of a sample of C18-MePh recrystallised from THF (red line), after being tempered at 84 °C (blue line), and after being rapidly crystallised from the melt (black line),

demonstrating the ability to increase the phase purity by subjecting the material to different thermal treatments.

5. References

1. Aragão, D.; Aishima, J.; Cherukuvada, H.; Clarken, R.; Clift, M.; Cowieson, N. P.; Ericsson, D. J.; Gee, C. L.; Macedo, S.; Mudie, N. MX2: A High-Flux Undulator Microfocus Beamline Serving Both the Chemical and Macromolecular Crystallography Communities at the Australian Synchrotron. *Journal of synchrotron radiation* **2018**, *25* (3), 885–891.
2. McPhillips, T. M.; McPhillips, S. E.; Chiu, H.-J.; Cohen, A. E.; Deacon, A. M.; Ellis, P. J.; Garman, E.; Gonzalez, A.; Sauter, N. K.; Phizackerley, R. P. Blu-Ice and the Distributed Control System: Software for Data Acquisition and Instrument Control at Macromolecular Crystallography Beamlines. *Journal of synchrotron radiation* **2002**, *9* (6), 401–406.
3. Kabsch, W. Automatic Processing of Rotation Diffraction Data from Crystals of Initially Unknown Symmetry and Cell Constants. *Journal of applied crystallography* **1993**, *26* (6), 795–800.
4. Sheldrick, G. M. Crystal Structure Refinement with SHELXL. *Acta Crystallographica Section C: Structural Chemistry* **2015**, *71* (1), 3–8.
5. Sheldrick, G. M. SHELXT–Integrated Space-Group and Crystal-Structure Determination. *Acta Crystallographica Section A: Foundations and Advances* **2015**, *71* (1), 3–8.
6. Dolomanov, O. V.; Bourhis, L. J.; Gildea, R. J.; Howard, J. A.; Puschmann, H. OLEX2: A Complete Structure Solution, Refinement and Analysis Program. *Journal of Applied Crystallography* **2009**, *42* (2), 339–341.
7. Piper, S. L.; Forsyth, C. M.; Kar, M.; Gassner, C.; Vijayaraghavan, R.; Mahadevan, S.; Matuszek, K.; Pringle, J. M.; MacFarlane, D. R. Sustainable Materials for Renewable Energy Storage in the Thermal Battery. *RSC Sustain.* **2023**. DOI: 10.1039/D2SU00111J